The Astrophysical Journal, 915:128 (11pp), 2021 July 10 https://doi.org/10.3847/1538-4357/ac02bf

Monte Carlo Investigation of the Ratios of Short-lived Radioactive Isotopes in the Interstellar Medium

Andrés Yagüe López[1,4], Benoit Côté[1,2,4], and Maria Lugaro[1,2,3]
[1] Konkoly Observatory, Research Centre for Astronomy and Earth Sciences, Eötvös Loránd Research Network (ELKH), Konkoly Thege Miklos ut 15-17, H-1121 Budapest, Hungary; andres.yague@csfk.hu
[2] ELTE Eötvös Loránd University, Institute of Physics, Budapest 1117, Pázmány Péter sétány 1/A, Hungary
[3] Monash Centre for Astrophysics, School of Physics and Astronomy, Monash University, VIC 3800, Australia
Received 2021 February 10; revised 2021 May 13; accepted 2021 May 17; published 2021 July 16

Abstract

Short-lived radioactive nuclei (SLR) with mean lives below ∼100 Myr provide us with unique insights into current galactic nucleosynthetic events, as well as events that contributed to the material of our solar system more that 4.6 Gyr ago. Here we present a statistical analysis of the ratios of these radioactive nuclei at the time of the early solar system (ESS) using both analytical derivations and Monte Carlo methods. We aim to understand the interplay between the production frequency and the mean lives of these isotopes, and its impact on their theoretically predicted ratios in the interstellar medium. We find that when the ratio of two SRLs, instead of the ratios of each single SLR relative to its stable or long-lived isotope, is considered, not only are the uncertainties related to the galactic chemical evolution of the stable isotope completely eliminated, but the statistical uncertainties are also much lower. We identify four ratios, ^{247}Cm/^{129}I, ^{107}Pd/^{182}Hf, ^{97}Tc/^{98}Tc, and ^{53}Mn/^{97}Tc, that have the potential to provide us with new insights into the *r*-, *s*-, and *p*-process nucleosynthesis at the time of the formation of the Sun, and need to be studied using variable stellar yields. Additionally, the latter two ratios need to be better determined in the ESS to allow us to fully exploit them to investigate the galactic sites of the *p* process.

Unified Astronomy Thesaurus concepts: Abundance ratios (11); Interstellar abundances (832); Meteorites (1038); Solar system formation (1530)

1. Introduction

Short-lived radioactive nuclei (SLR) are unstable nuclei with mean lives ≈0.1 to 100 Myr. Their abundances can be measured in a variety of locations, both live via γ-ray spectroscopy (Diehl et al. 2010) and analysis of deep-sea sediments (Wallner et al. 2015), and extinct, as in the case of their early solar system (ESS) abundances inferred through the excess of their daughter nuclei in meteoritic samples (Dauphas & Chaussidon 2011). Because of their short mean lives relative to the age of the Galaxy, these nuclei represent the fingerprint of current nucleosynthesis, some of them do not even live long enough to travel far away from their site of origin, which results in the decoupling of their abundances from galaxy-wide mixing processes (see, e.g., Diehl et al. 2010; Fujimoto et al. 2018). When their evolution in the Galaxy is considered, SLRs therefore probe the current galactic star formation rate instead of the star formation history (Clayton 1984; Meyer & Clayton 2000; Huss et al. 2009), and as such, they are relatively unaffected by the processes that operate over the full timescale of the Galaxy, such as galactic inflows and outflows (e.g., Somerville & Davé 2015; Naab & Ostriker 2017; Tumlinson et al. 2017), the buildup of the total stellar mass (e.g., Bland-Hawthorn & Gerhard 2016), and the mixing and recycling processes (e.g., Anglés-Alcázar et al. 2017). These sources of uncertainty instead significantly affect the stable or long-lived reference isotope used to measure the abundance of SLR nuclei in the ESS. In Côté et al. (2019a), we considered the impact of these sources of uncertainty on the determination of radioactive-to-stable isotopic ratios in the Galaxy and derived that their impact on the ratio results in a variation of a factor of 3.5 at most.

There are other sources of uncertainty, however, that must be considered for the evolution of SLRs in the interstellar medium (ISM). As mentioned above, due to their short mean life, SLRs are not evenly distributed in the Galaxy (Fujimoto et al. 2018; Pleintinger et al. 2019). In particular, the evolution of an SLR at a specific location in the Galaxy directly depends on the ratio of its mean life τ and the average time between enriching events $\langle\delta\rangle$, as well as on the specific statistical distribution of these δ (see Côté et al. 2019b, henceforth Paper I). The reason for this can be understood by analyzing two limiting cases: $\tau \gg \langle\delta\rangle$ and $\tau \ll \langle\delta\rangle$. In the first case, the mean life is much longer than the time between two enriching events. This allows for the buildup of a memory[5] of the SLR abundance up to a steady-state (between production and decay) equilibrium value equal to the yield of a single event multiplied by a factor $\tau/\langle\delta\rangle$. In the second case, the expected time between two enriching events is instead far enough apart to allow for the complete decay of the SLR before the next event, leaving almost no memory. In this case, the average abundance therefore remains below the value of the yield. In relation to investigations of the ESS, the first case allows us to calculate the isolation time ($T_{\rm iso}$), defined as the time between the decoupling of the material that ended up in the solar nebula from the Galactic chemical enrichment processes (in other words, the birth of the colder and denser molecular cloud) and the formation of the first solids in the nebula. The second case instead allows us to calculate the time from the last event ($T_{\rm LE}$), defined as the time since the last nucleosynthesis event in the Galaxy that contributed a particular SLR to the solar system matter (Lugaro et al. 2014, 2018). If $T_{\rm LE}$ can be calculated, then the SLR may

[4] NuGrid Collaboration,http://nugridstars.org.

[5] Here we define memory as the SLR abundance remains, nondecayed, from the enrichment events that occurred before the last event.

also be used as constraints for the features of specific nucleosynthetic events (see Côté et al. 2021).

In Paper I we analyzed the SLR abundance distribution resulting from an uneven temporal distribution of a nucleosynthetic source, and derived the uncertainties due to this temporal granularity of the enriching events using a simple statistical model of a given region in the Galaxy affected by several enriching events via a Monte Carlo calculation. We concluded that the interplay of the time between two enriching events and the mean life of the SLR determines both the steady-state equilibrium value and its uncertainty. The uncertainty calculated in Paper I does not affect the abundance of the stable reference nucleus, which is well mixed within 100 Myr (e.g., de Avillez & Mac Low 2002), and can be simply composed with the uncertainty due to the galactic chemical evolution (GCE) studied by Côté et al. (2019a) to calculate the total uncertainty in the SLR/stable isotopic ratio. This total uncertainty can then be used to deduce information about the isolation time (see Paper I, Section 5) or the time since the last enriching event (see Côté et al. 2021).

Here, we use the same methodology as in Paper I to study the effect of the presence of heterogeneities due to the temporal granularity of their stellar sources on the behavior and uncertainty of the ratio of two SLRs. This ratio can exhibit a markedly different behavior to that of a SLR/stable isotope ratio because its evolution also depends on the difference between the two mean lives. We restrict ourselves to analyzing the scenario of synchronous enrichment scenario. That is, the situation in which both SLRs are always generated in the same events. This means that the evolutions of the abundances of both isotopes are correlated, and the uncertainty of their ratio cannot be simply derived by adding the individual abundance uncertainties on each isotope. We also assume that the production ratio P of the two SLRs is always the same. The extension to a more general framework in which different events have different production ratios will not fundamentally change our conclusions as long as both isotopes are always created together. We do not analyze instead the complementary asynchronous enrichment scenario, where at least one of the SLRs is created in more than one type of event. This scenario is more complex to analyze with our statistical method because it is not possible to define a single production ratio for this case. Furthermore, the possibility that the two SLR may have different $\langle\delta\rangle$ values from different sources complicates the general analysis.

The outline of the paper is as follows. In Section 2 we assume that δ is constant and present the analytical solutions to quantify the abundance and uncertainty of any ratio involving two SLRs for four different regimes. In Section 3 we extend our analysis by accounting for a variable δ and run Monte Carlo calculations to better quantify the uncertainty on SLR abundance ratios. In Section 4 we apply our statistical framework to radioactive isotopic ratios relevant for the ESS and discuss the implication of our work on the derivation of $T_{\rm iso}$ and $T_{\rm LE}$. The codes used in this work are publicly available on GitHub.[6]

2. The Case of $\delta = \delta_c =$ Constant

We start with the analysis of the simplest case, which assumes that the time between enriching events δ is constant. The steady-state abundance (in mass) of a single SLR with mean life τ is

$$M = M_{\rm ej}\frac{1}{1 - e^{-\delta_c/\tau}}e^{-\Delta t/\tau}, \quad (1)$$

where $M_{\rm ej}$ is the ejected mass from a single event, δ_c is the constant time between two successive enrichments, and $\Delta t < \delta_c$ is the time since the last enrichment (see Lugaro et al. 2018).

By taking Equation (1) for two isotopes M_1 and M_2 with mean lives τ_1 and τ_2, respectively, the steady-state evolution of their ratio can be described as

$$\frac{M_1}{M_2} = P\,\frac{1 - e^{-\delta_c/\tau_2}}{1 - e^{-\delta_c/\tau_1}}e^{-\Delta t/\tau_{\rm eq}}, \quad (2)$$

where P is the production ratio at the stellar source, and $\tau_{\rm eq}$ is the equivalent mean life given by

$$\tau_{\rm eq} = \frac{\tau_1\tau_2}{\tau_2 - \tau_1}, \quad (3)$$

and representing the mean life of the ratio of the radioactive isotopes. Note that $\tau_{\rm eq}$ can be negative if $\tau_1 > \tau_2$. Although we generally consider the case where $\tau_{\rm eq}$ is positive, we explain the differences with the negative case wherever they exist.

The time-averaged value of Equation (2) is given by (see the Appendix)

$$\left\langle\frac{M_1}{M_2}\right\rangle = \mu = P\,\frac{\tau_{\rm eq}}{\delta_c}\,\frac{1 - e^{-\delta_c/\tau_2}}{1 - e^{-\delta_c/\tau_1}}(1 - e^{-\delta_c/\tau_{\rm eq}}), \quad (4)$$

and the difference between its maximum and minimum (derived by taking $\Delta t = 0$ and $\Delta t = \delta_c$ in Equation (2)) values can be written as

$$\mathrm{Max} - \mathrm{Min} = \mu\frac{\delta_c}{\tau_{\rm eq}}. \quad (5)$$

Equation (4) is remarkably similar to that derived in Lugaro et al. (2018) for an SLR/stable isotopic ratio, with the main difference being that the mean life of the radioactive isotope τ is now substituted by the mean life of the ratio of the radioactive isotopes $\tau_{\rm eq}$, and that now the multiplying exponentials do not cancel out.[7] The relative variation, that is, the difference between the maximum and minimum value divided by the average, is otherwise identical to the case of the SLR/stable isotopic ratio, provided we substitute the SLR mean life with the equivalent mean life. This means that qualitatively, we can expect the uncertainty of the ratio between two radioactive isotopes to behave like that of a single radioactive isotope with a mean life given by $\tau_{\rm eq}$. However, the fact that the average value contains three nonvanishing exponentials means that depending on the relative values of δ_c, τ_1, τ_2, and $\tau_{\rm eq}$, we face four qualitatively distinct regimes for the evolution of the ratio itself. These regimes are exemplified in Figure 1 and explained below.

2.1. Regime 1: $\delta_c \gg \tau_{eq}$, τ_1, τ_2

We study first the regime where $\delta_c \gg \tau_{\rm eq}$, τ_1, τ_2. In this case, represented by the example in the top left panel of Figure 1, the

[6] https://github.com/AndresYague/Stochastic_RadioNuclides

[7] When only one radioactive isotope at the numerator is considered, there is no exponential with τ_2 at the numerator, and $\tau_{\rm eq} = \tau_1$, leaving just τ/δ_c.

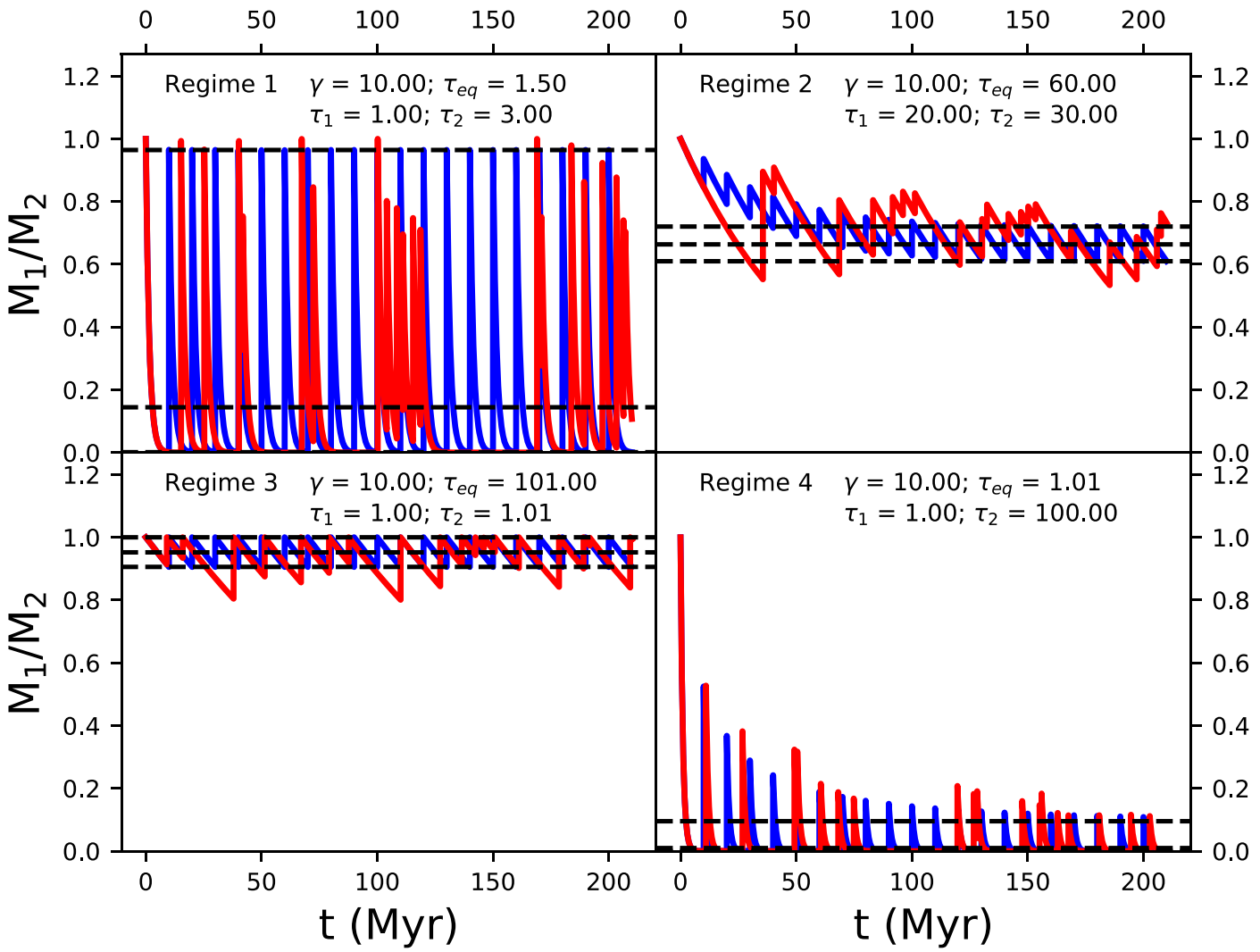

Figure 1. Examples of the behavior of the four regimes explored in this work when $\tau_{eq} > 0$. The production ratio P is taken to be 1. The blue lines are the evolution for constant delta δ_c, and the dashed black lines correspond to the maximum, average, and minimum values given by Equations (4) and (5), while the red lines are the evolution when δ is a random variable. In the figure annotation, γ represents the time between the formation of two enrichment source progenitors instead of the time between two actual successive enrichment events, exactly as defined in Paper I. As in that work, we find that $\gamma = \langle\delta\rangle$. The larger uncertainty of the stochastic case relative to the δ_c case is readily apparent for all of the regimes.

average abundance ratio is

$$\mu = \begin{cases} \dfrac{\tau_{eq}}{\delta_c} P & \text{if } \tau_{eq} > 0, \\ \dfrac{|\tau_{eq}|}{\delta_c} P\, e^{\delta_c/|\tau_{eq}|} & \text{if } \tau_{eq} < 0. \end{cases} \quad (6)$$

Given that the ratio τ_{eq}/δ_c is low, we expect an average value much lower than the production ratio P when $\tau_{eq} > 0$. For a case where $\tau_{eq} < 0$, we have an exponential term of $\delta_c/|\tau_{eq}|$, which will instead yield an average value much higher than P. In addition, the ratio will vary between the production ratio P and 0 (or P and $P\exp(\delta_c/|\tau_{eq}|)$) for the case of positive (negative) τ_{eq}.

The intuitive understanding of this regime is that the time between enrichment events is longer than it takes for both radioactive isotopes and their ratio to decay, which prevents any memory buildup and results in a very large relative uncertainty.

2.2. Regime 2: $\delta_c \ll \tau_{eq}$, τ_1, τ_2

In this regime, $\delta_c \ll \tau_{eq}$, τ_1, τ_2. This case, represented in the top right panel of Figure 1, has an average equilibrium value of

$$\mu = P\,\frac{\tau_1}{\tau_2}. \quad (7)$$

The evolution of the ratio of radioactive isotopes is marked by relatively frequent events, and the time between them is shorter than the mean life of any of the isotopes. This means that the abundance of both isotopes retains the memory of the previous events, and the ratio drifts from the production ratio P to oscillate around the equilibrium average with a low relative uncertainty, behaving in a similar fashion to the case of large τ/δ_c studied in Lugaro et al. (2018).

2.3. Regime 3: $\delta_c \ll \tau_{eq}$ and $\delta_c \gg \tau_1$, τ_2

In this regime, $\delta_c \ll \tau_{eq}$ and $\delta_c \gg \tau_1$, τ_2. This case, represented in the bottom left panel of Figure 1, has an average equilibrium

value of

$$\mu = P. \tag{8}$$

Although the value for the average in this case can be recovered from the formula of Regime 2 by using $\tau_1 \approx \tau_2$, we set this case apart because it represents the specific situation when the equivalent mean life is much longer than δ_c, while the individual mean lives of each isotope are not. This regime only arises when the difference between the mean lives is small enough to make $\tau_{\rm eq}$ orders of magnitude longer than them (see Equation (3)). Given the short mean life of the individual SLR, it is likely that each SLR carries information from the last event alone (see Paper I, Figure 9 and the related discussion). At the same time, the variation on the value of the ratio is relatively small because the equivalent mean life is too long for the ratio to change significantly before the next enriching event.

2.4. Regime 4: $\delta_c \gg \tau_{eq}$, τ_1; $\delta_c \ll \tau_2$

In this regime, $\delta_c \gg \tau_{\rm eq}$, τ_1, but $\delta_c \ll \tau_2$. The average value in this case, shown in the bottom right panel of Figure 1, is

$$\mu = \begin{cases} \dfrac{\tau_{\rm eq}}{\tau_2} P & \text{if } \tau_{\rm eq} > 0, \\ \dfrac{|\tau_{\rm eq}|\tau_1}{\delta_c^2} e^{\delta_c/|\tau_{\rm eq}|} P & \text{if } \tau_{\rm eq} < 0. \end{cases} \tag{9}$$

Although the evolution resembles that of the first regime when $\tau_{\rm eq} > 0$, the maximum value attained by the ratio of the radioactive isotopes in the equilibrium becomes much lower than P. The reason is that although the evolution of M_1 does not retain the memory of the previous events, the evolution of M_2 does. We note that in this regime, $\tau_{\rm eq} \approx \min(\tau_1, \tau_2)$.

3. The Case of the Variable δ

The cases studied in the previous section for a constant δ provide indicate how the ratio of two radioactive isotopes can behave in general. However, this simple approach produces deceptively small uncertainties relative to the more realistic scenario of the variable δ. This situation has been explored in Paper I for the case of the evolution of a single radioactive isotope, and it is illustrated here in Figure 1 for the case of the ratio of two radioactive isotopes as well. To gain a better representation of SLR abundance variations in the ISM, we turn to a Monte Carlo approach in which the enriching rate is stochastic, as in Paper I.

The setup for the Monte Carlo experiments is the same as in Paper I. A total of 1000 runs are calculated for 15 Gyr each. For each run, the progenitors of the enriching events are generated with a constant time interval of γ. The time between the birth of the progenitor and the associated enriching event is sampled from a source-specific delay-time distribution (DTD). The enriching times are sorted and the random δ calculated from their consecutive differences (see Figure 2 of Paper I). Because the value for $\langle\delta\rangle$ is approximately that of γ, we use the terms interchangeably in this work.

The DTDs used here have an equal probability between given initial and final times, and are the same as the "box" DTD of Paper I. We have omitted the power-law DTD because as we concluded in Paper I, the actual δ distribution is approximately the same for both types of DTD for equal initial and final times. As in Paper I, we refer to the uniform

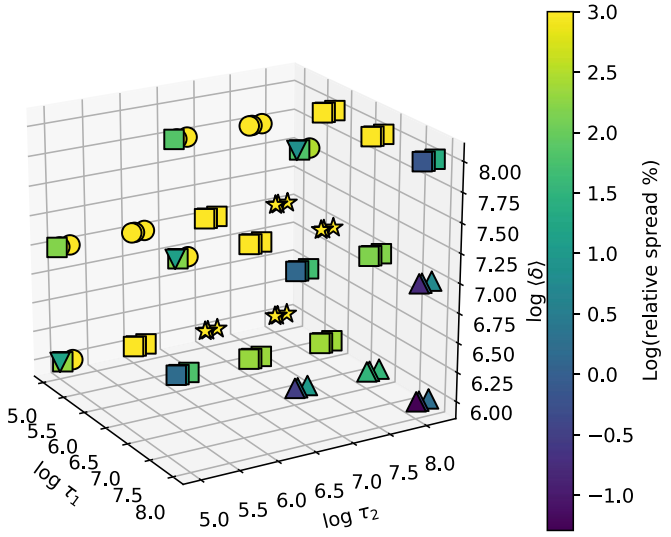

Figure 2. Dependence of the relative spread around the median on τ_1, τ_2, and $\langle\delta\rangle$. The four different regimes illustrated in Figure 1 cluster with different regions in this plot. Regimes 1 (circles) and 4 (stars) are located in the upper and lower left far corner, respectively, with a logarithmic relative spread values above 2 dex (100%). Regime 2 (triangles) is located in the lower right far corner, with a logarithmic relative spread values between 0 (1%) and 1.5 dex (32%), and Regime 3 (inverted triangles) is located on the diagonal contained in the $\tau_1 \approx \tau_2$ plane, with a logarithmic relative spread lower than 1 dex. Cases with the same $\tau_{\rm eq}$ correspond to vertical lines with constant τ_1 and τ_2. Squares represent combinations that do not fall neatly into any regime and often correspond to a transition between two regimes.

distribution between 3 and 50 Myr, 50 Myr and 1 Gyr, and 50 Myr and 10 Gyr as the "short," "medium," and "long" box DTD, respectively. Each of these boxes can be associated with a different type of progenitor for the enriching event, as described in Paper I.

Because in the synchronous case, both radioisotopes are generated in the same events, the ratios are computed at each time step for the same run. To explore the different regimes, each of the 1000 runs is repeated using different τ. We consider 1000 runs to be enough for the same reasons as in Paper I: different temporal points of different runs are statistically independent and can therefore be considered as different experiments for the purposes of statistical derivation. For this reason, we stack together all the values between 10 and 14 Gyr to represent the final distribution of M_1/M_2. All the cases studied here have $\tau_1 < \tau_2$. This particular choice is arbitrary, but cases with $\tau_1 > \tau_2$ result in positive exponential behavior, and the abundance ratio is no longer bounded and can diverge toward infinity, which complicates the analysis without adding any meaning.

In Figure 2 we show the relative uncertainty (68.2% of the distribution around the median of the ratio) resulting from the Monte Carlo experiments when τ_1, τ_2, and γ are varied. As the figure shows, Regimes 1 and 4 have extremely large relative uncertainties, mainly because M_1 does not build up sufficient memory. Therefore these regimes can only be treated as additions of individual events, using statistical methods different from that used here. This is similar to the case of Regime II of Paper I (all the regimes of Paper I and their connections to the present regimes are described in more detail in Section 3.1). From now on, we therefore focus on the cases where $\tau_{\rm eq} \gtrsim 3\langle\delta\rangle$, which excludes Regimes 1 and 4. The exception is Regime 3, where although neither M_1 nor M_2 build up enough memory from previous events, the slowly decaying

Table 1
Median Values and 68% Confidence Interval for Cases Belonging to Regime 2 and Lower Limits Encompassing 84% of the Distribution for Cases Belonging to Regime 3 from the Monte Carlo Experiment (for $P = 1$) for Different Values of γ, τ_1/γ, τ_2/γ, and τ_{eq}/γ for $\tau_{eq}/\gamma > 3$

γ (Myr)	τ_1/γ	τ_2/γ	τ_{eq}/γ	Small Box	Large Box	Regime
1.00	0.10	0.10	10.10	>0.83	>0.83	3
1.00	1.00	1.01	101.00	>0.98	>0.98	3
1.00	1.00	1.10	11.00	>0.80	>0.80	3
1.00	1.00	1.50	3.00	$0.63^{+0.13}_{-0.20}$	$0.63^{+0.13}_{-0.20}$	–
1.00	10.00	10.10	1010.00	$0.99^{+0.00}_{-0.00}$	$0.99^{+0.00}_{-0.00}$	2
1.00	10.00	11.00	110.00	$0.91^{+0.01}_{-0.01}$	$0.91^{+0.01}_{-0.02}$	2
1.00	10.00	15.00	30.00	$0.66^{+0.03}_{-0.04}$	$0.66^{+0.04}_{-0.04}$	2
1.00	10.00	101.00	11.10	$0.10^{+0.02}_{-0.02}$	$0.10^{+0.02}_{-0.02}$	2
1.00	10.00	110.00	11.00	$0.09^{+0.02}_{-0.01}$	$0.09^{+0.02}_{-0.02}$	2
1.00	10.00	150.00	10.71	$0.07^{+0.01}_{-0.01}$	$0.07^{+0.01}_{-0.01}$	2
1.00	100.00	101.00	10100.00	$0.99^{+0.00}_{-0.00}$	$0.99^{+0.00}_{-0.00}$	2
1.00	100.00	110.00	1100.00	$0.91^{+0.00}_{-0.00}$	$0.91^{+0.00}_{-0.00}$	2
1.00	100.00	150.00	300.00	$0.67^{+0.01}_{-0.01}$	$0.67^{+0.01}_{-0.01}$	2
10.00	0.10	0.10	10.10	>0.86	>0.83	3
10.00	1.00	1.01	101.00	>0.98	>0.98	3
10.00	1.00	1.10	11.00	>0.83	>0.80	3
10.00	1.00	1.50	3.00	$0.64^{+0.12}_{-0.17}$	$0.63^{+0.13}_{-0.20}$	–
10.00	10.00	10.10	1010.00	$0.99^{+0.00}_{-0.00}$	$0.99^{+0.00}_{-0.00}$	2
10.00	10.00	11.00	110.00	$0.91^{+0.01}_{-0.01}$	$0.91^{+0.01}_{-0.01}$	2
10.00	10.00	15.00	30.00	$0.67^{+0.02}_{-0.02}$	$0.66^{+0.04}_{-0.04}$	2
100.00	0.10	0.10	10.10	$0.95^{+0.03}_{-0.03}$	>0.83	3
100.00	1.00	1.01	101.00	$0.99^{+0.00}_{-0.00}$	>0.98	3
100.00	1.00	1.10	11.00	$0.90^{+0.03}_{-0.03}$	>0.80	3
100.00	1.00	1.50	3.00	$0.65^{+0.08}_{-0.08}$	$0.63^{+0.13}_{-0.20}$	–

Note. The results from the large box are identical to those from the medium box DTD. A dash in the Regime column means that the specific case does not fall neatly into one of the regimes. These cases typically fall between Regimes 1 or 4 and Regime 3.

property of their ratio results in a stable value with a low relative uncertainty. This makes Regime 3 an interesting case where the uncertainty in the ratio of two SLR is as low or lower than in Regime 2, with a high percentage of the ratio containing only the abundances from the last event.

The uncertainties from the Monte Carlo calculations are presented in Table 1 for $\tau_{eq} > 0$ and $\tau_{eq}/\gamma > 3$. When the distribution is approximately symmetric (Regime 2), both an upper and lower value are given, when the distribution piles up on P (Regime 3), a lower limit for the ratio is given instead. Table 1 allows us to calculate uncertainties for ratios of the SLR due to the temporal stochasticity of enrichment events. For any isotopic ratio, we can select the proper γ, which depends on the source, the best-suited τ_1/γ and τ_2/γ, and whether a short box (i.e., if the source is a core-collapse supernovae) or a long box (i.e., if the source is an asymptotic giant branch star or a neutron star merger) describes the source. Afterward, the corresponding numbers in Column 5 or 6 should be multiplied by the production ratio of the SLR ratio. If there is no exact match to the numbers shown in Table 1, then Equations (10) and (11) or (13) described below in Section 3.2 can be used instead. In Sections 3.3 and 3.4, we describe in more detail the differences between the constant and random δ cases in relation to Regimes 2 and 3, respectively.

3.1. Connections and Similarities with the Regimes Defined in Paper I

In Paper I we analyzed a single SLR and found that three different regimes can be applied depending on the relation between τ and γ. Here we report a brief description of them and and how they connect with the regimes in this work. For the sake of clarity, the three regimes from Paper I are marked in Roman numerals, while Arabic numerals refer to the four regimes considered here.

Regime I refers to $\tau/\gamma > 2$ and is similar to Regimes 2 or 3 in that statistics can be calculated because the spread is not much larger than the median value. Regime I is associated with the calculation of the isolation time, T_{iso}, because in this case, the ISM will contain an equilibrium value from where there can be an isolation period before the ESS abundances. In the present work, Regime 2 is that associated with the calculation of T_{iso}.

Regime III is a case that covers the region of $\tau/\gamma < 0.3$. In this regime, there is a high probability that the ISM abundance that decayed into the ESS abundance originated from a single event. Therefore this regime is associated with the calculation of the time since the last event, T_{LE}. Regime 3 of this work is related to Regime III of Paper I in that both most likely carry abundances from only the last event before the formation of the solar system. The difference is that while Regime III allows us to calculate T_{LE}, Regime 3 also allows us to narrowly determine the production ratio of the last event.

Regime II falls between two well-defined cases described above. This regime has $0.3 < \tau/\gamma < 2$, which does not allow for meaningful statistics nor for a clean definition of a last event to which the ISM abundance can be solely or mostly attributed. This regime does not correspond to any of the regimes in this work, and it may be similar to the region between Regime 2 and Regimes 1 and 4.

3.2. Analytical Approach

We also investigated the possibility of calculating the uncertainties using an analytical approach instead of the full Monte Carlo simulations. The aim is to provide a better understanding of the regimes and their uncertainties, as well as give an alternative to calculating approximate numbers without the need of a simulation. To do this, we use the expression for the average given by

$$\mu \approx P \frac{\tau_{\rm eq}}{\langle\delta\rangle} \frac{1-\langle e^{-\delta/\tau_2}\rangle}{1-\langle e^{-\delta/\tau_1}\rangle}(1-\langle e^{-\delta/\tau_{\rm eq}}\rangle), \quad (10)$$

derived in the Appendix, and for the relative standard deviation, we use

$$\frac{\sigma}{\mu} \approx F\sqrt{\frac{\langle\delta\rangle}{2\tau_{\rm eq}} \frac{1-\langle e^{-2\delta/\tau_{\rm eq}}\rangle}{(1-\langle e^{-\delta/\tau_{\rm eq}}\rangle)^2} - 1}, \quad (11)$$

where F is a correction factor applied to Equation (A14) and is defined by

$$F = K\left[1+\log_{10}\left(\frac{\min(\tau_1,\tau_2)}{\langle\delta\rangle}\right)^2\right], \quad (12)$$

where $K=1$ unless $\min(\tau_1, \tau_2)$ is larger than the span of the DTD, in which case, $K=0.5$. In cases where $\min(\tau_1, \tau_2) < \langle\delta\rangle$, then $F=K$.

This factor F was derived from the Monte Carlo experiments and corrects some of the approximations made in the derivation of A14 in the Appendix. With this correction factor, Equation (11) becomes an accurate estimate of the results of the Monte Carlo experiment.

If the full distribution of δ is unknown, a further approximation to Equation (11) can be used instead, rendering

$$\frac{\sigma}{\mu} \approx F\sqrt{\frac{1}{6}\frac{\langle\delta\rangle^3+3\sigma_\delta^2\langle\delta\rangle}{\tau_{\rm eq}^2\langle\delta\rangle-\tau_{\rm eq}\sigma_\delta^2}}, \quad (13)$$

with the advantage that only $\langle\delta\rangle$ and σ_δ (the standard deviation of the delta distribution) have to be known. This formula is much easier to calculate because no sampling of the δ distribution is needed.

The validity of Equations (11) and (13) can be tested by comparing them to the 68.2% (1σ) confidence interval calculated from the Monte Carlo experiments. This comparison is presented in Figure 3. In the worst case, with the small-box DTD, the relative difference between the analytical approximations, and the results from the numerical experiments are just above 25%. These are valid for calculations related to Regime 2. For Regime 3, as seen in Table 1, the average instead remains very close to P and introduces asymmetry in the distribution. In this case, the theoretical σ is an average of the lower and upper 1σ threshold. When this σ is such that $\mu+\sigma > P$, it is better to calculate a lower limit for the distribution with $P-2\sigma$ because in this case, the distribution piles up at P, making any value between P and μ functionally equiprobable.

3.3. Regime 2: $\delta \ll \tau_{eq}$, τ_1, τ_2

In this case, the abundances of both SLR nuclei retain significant memory from past events. The average of their ratio, according to Equation (10), is the same as the constant case for the same regime, given by Equation (7). When the uncertainties are compared, however, there is a significant difference between the constant and the stochastic case. As a first-order approximation, and taking $\sigma_\delta \approx \langle\delta\rangle$ (see Table 2 of Paper I), we can write Equation (13) as

$$\frac{2\sigma}{\mu} \approx 2F\frac{\langle\delta\rangle}{\tau_{\rm eq}}, \quad (14)$$

which, when $\langle\delta\rangle$ is substituted by δ_c and Equation (12) is divided by Equation (5), reveals that the stochastic case has a larger uncertainty relative to the constant case by a factor of 2F. This factor can be shown to be in the range $2F \in [2.5, 35]$ when we consider $\tau_{\rm eq}/\langle\delta\rangle \in [3, 10^4]$ by using Equation (12) with $K=1$ and take $\min(\tau_1, \tau_2) = \tau_{\rm eq}$. Therefore the time-stochastic nature of enrichment events can increase the uncertainty by more than an order of magnitude in this regime. The uncertainty on the ratio of two SLR in Regime 2 is still relatively low. For example, for the large box, with $\tau_1 = 10$ Myr, $\tau_2 = 15$ Myr, and $\gamma = 1$ Myr, Table 1 has a relative uncertainty of 12%. For a similar example with $\tau = 10$ Myr and $\gamma = 1$ Myr in Table 3 of Paper I, the relative uncertainty is 45% for the large box. Even if we take the case of $\tau = 31.6$ Myr and $\gamma = 1$ Myr, we still have a relative uncertainty of 25% for the SLR/stable isotopic ratio.

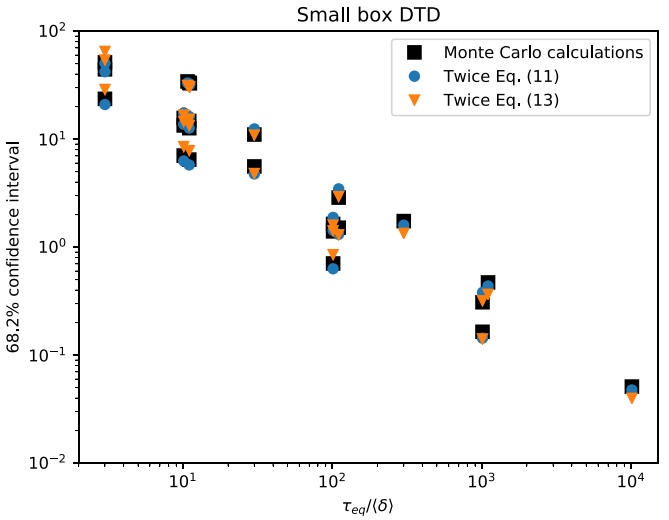

Figure 3. Prediction of Equations (11) and (13) of the relative to the median 68.2% confidence interval calculated from the Monte Carlo experiments (large black squares) for the small-box DTD. The equations themselves calculate just the 34.1% interval, which is why twice their value is used.

3.4. Regime 3: $\delta \gg \tau_{eq}$, τ_1, τ_2

As discussed in the constant δ_c scenario, this regime shows a low variation around the average P while retaining no memory of previous events. The difference between the constant and stochastic case is similar to that in Regime 2 (because Equation (13) only depends on $\langle\delta\rangle$ and $\tau_{\rm eq}$), that is, a factor of $2F$. The factor $F=K$ is a constant here (when $\min(\tau_1, \tau_2) < \langle\delta\rangle$), equal either to 0.5 or to 1, which means that the relation between the uncertainties in the constant and stochastic cases is a factor of two at most. Additionally, the stochastic case results in a nonsymmetric distribution around the median. The reason is that the ratio is always bounded between 0 and the production factor P (when $\tau_2 > \tau_1$): when the enriching events are more frequent than average, the ratio will remain at P, while when the enriching

Table 2
Regimes and Values of the Ratios from the Monte Carlo (MC) Experiments Applied to the Specific Cases of Ratios of Two SLRs (Column SRL_1/SRL_2) and of the SLRs and Their Corresponding Stable or Long-lived Reference Isotopes (Columns SRL_1/stable and SRL_2/stable, See the Main Text for the List of Reference Isotopes)

	τ_1	τ_2	τ_{eq}	γ	SLR_1/stable		SLR_2/stable		SLR_1/SLR_2	
					Regime	MC Values	Regime	MC Values	Regime	MC Values
$^{247}Cm/^{129}I$	22.5	22.6	5085	1	I	$22.37^{+3.45}_{-3.22}$	I	$22.47^{+3.46}_{-3.23}$	2	$1.00^{+0.00}_{-0.00}$
				3.16	I	$7.01^{+1.98}_{-1.77}$	I	$7.04^{+1.99}_{-1.77}$	2	$1.00^{+0.00}_{-0.00}$
				10	II	<3.29	II	<3.30	3	$1.00^{+0.00}_{-0.00}$
				31.6	II	<1.29	II	<1.29	3	>0.99
				100	III	<0.54	III	<0.54	3	>0.96
				316	III	<0.08	III	<0.08	3	>0.89
$^{107}Pd/^{182}Hf$	9.4	12.8	35.4	1	I	$9.28^{+2.27}_{-2.05}$	I	$12.68^{+2.63}_{-2.41}$	2	$0.73^{+0.03}_{-0.04}$
				3.16	I	$2.86^{+1.32}_{-1.10}$	I	$3.94^{+1.53}_{-1.31}$	2	$0.73^{+0.06}_{-0.08}$
				10	II	<1.62	II	<2.06	3	$0.70^{+0.12}_{-0.19}$
				31.6	III	<0.69	III	<0.86	–	$0.50^{+0.30}_{-0.32}$
$^{53}Mn/^{97}Tc$	5.4	5.94	59.4	1	I	$5.29^{+1.75}_{-1.53}$	I	$5.83^{+1.83}_{-1.61}$	2	$0.91^{+0.02}_{-0.02}$
				3.16	II	<2.63	II	<2.84	3	$0.90^{+0.03}_{-0.05}$
				10	II	<1.04	II	<1.12	3	$0.86^{+0.08}_{-0.15}$
				31.6	III	<0.41	III	<0.45	–	$0.68^{+0.22}_{-0.31}$
$^{97}Tc/^{98}Tc$	5.94	6.1	226	1	I	$5.83^{+1.83}_{-1.61}$	I	$5.99^{+1.85}_{-1.63}$	2	$0.97^{+0.00}_{-0.01}$
				3.16	II	<2.84	II	<2.91	3	$0.97^{+0.01}_{-0.02}$
				10	II	<1.12	II	<1.14	3	$0.96^{+0.02}_{-0.05}$
				31.6	III	<0.45	III	<0.47	3	$0.90^{+0.07}_{-0.13}$
				100	III	<0.05	III	<0.06	–	$0.73^{+0.19}_{-0.29}$

Note. Production ratios are always 1. Also indicated are τ_1, τ_2, τ_{eq}, and the adopted γ, all in Myr. The values of γ are selected such that it is possible to remain within Regimes 2 or 3, for which cases we can model the uncertainties. The Roman numerals correspond to the regimes of Paper I ($SRL_{1,2}$/stable), while the Arabic numerals correspond to the regimes described in this work. The dashes correspond to cases that do not fit neatly in any of the regimes.

events are less frequent than average, the ratio decays away from this average. In any case, the characteristic of Regime 3 is that the average ratio always remains very close to P.

4. Discussion

We apply our general theoretical approach to the specific ratios of two SLRs that are either in Regime 2 or Regime 3. Starting from Table 2 of Lugaro et al. (2018), which lists all the SLRs known to have been present in the ESS, we select SLRs with potentially the same origin (for the synchronous scenario) and with mean lives close enough such that the τ_{eq} of their ratio is potentially longer than the probable γ of their source. We find four cases of such ratios of isotopes and present them in Table 2, along with the specific Monte Carlo experiments that reproduce the conditions under which they evolve in the Galaxy, assuming a production ratio $P = 1$. This table categorizes the regime of the selected SLR ratios, realizes the difference with regard to the uncertainties between considering the single SLR/stable (or long-lived) reference isotope ratio (Columns SLR_1 and SLR_2), and quantifies the ratio of the two SLRs (Column SLR_1/SLR_2). In general, the uncertainties significantly decrease when ratios of SLRs with similar mean lives are considered compared to when their ratio to a stable or long-lived isotope is considered (compare the last column of Monte Carlo values to the other two columns of Monte Carlo values). It is worth mentioning that in this comparison we assume that the stable isotope carries no uncertainty at all from GCE processes, which by itself can be a factor of up to $5.7/1.6 = 3.6$ (Côté et al. 2019a). In addition, the predicted ISM abundances are much closer to the production ratios when the ratios of two SLRs are considered.

Table 3 shows the subsequent calculations of the isolation time, T_{iso} (in roman), and the time since the last event, T_{LE} (in italics), for the selected isotopic ratios for which the ESS ratio is available. These correspond to only three out of the four ratios discussed in Table 2. We excluded $^{97}Tc/^{98}Tc$ because only upper limits are available for the corresponding radioactive-to-stable ratios, which means that it is not possible to derive any ESS value for their ratio. The other ESS ratios are calculated using the values for the radioactive-to-stable ratios reported in Table 2 of Lugaro et al. (2018) and the solar abundances of the reference isotopes from Lodders (2010; see also Côté et al. 2021). Furthermore, the selected values for γ were limited to those most likely to occur in the Milky Way for the corresponding production sites.

4.1. The Ratio of the r-process ^{247}Cm and ^{129}I

These two isotopes are made by the rapid neutron-capture (r) process, and typical estimates for the time interval at which r-process nucleosynthetic events that are believed to enrich a parcel of gas in the Galaxy range between 200 and 500 Myr (Hotokezaka et al. 2015; Tsujimoto et al. 2017; Bartos & Marka 2019; Côté et al. 2021). Therefore the case of $^{247}Cm/^{129}I$ is the best example of Regime 3 because $\tau_{eq} = 5085$ Myr (Table 2) is much longer than γ, while each τ ($\simeq$22.5 and 22.6 Myr, respectively) is much shorter than γ. The ratios to the long-lived or stable references isotopes, $^{247}Cm/^{235}U$ and $^{129}I/^{127}I$, allow us to derive a T_{LE}, for example, for the specific γ value of 316 Myr considered in Table 3, and derive typical production ratios of 1.35 for $^{129}I/^{127}I$ and 0.3 for $^{247}Cm/^{235}U$. While our T_{LE} values are not perfectly compatible with each other, the more

Table 3
Timescales Derived by Decaying the Reported ISM Ratios to the ESS Ratios in Column 2 for a Subset of Ratios and γ Values Considered in Table 2 to Represent Possible Realistic Values in the Galaxy for the Corresponding Production Event

	ESS Ratio	τ_{eq}	γ	SLR_1/stable		SLR_2/stable		SLR_1/SLR_2	
				ISM Ratio	Time	ISM Ratio	Time	ISM Ratio	Back-decayed Ratio
$^{247}Cm/^{129}I$	2.28×10^{-3}	5085	316	*9.63×10^{-2}*	*171*	*1.15×10^{-1}*	*153*	*1.22×10^{-2}*[a]	*2.35×10^{-3}*
$^{107}Pd/^{182}Hf$	4.25	35.4	1	3.56×10^{-4}	16^{+2}_{-3}	5.20×10^{-4}	21^{+2}_{-3}	*2.41*	*7.17*
			3.16		16^{+4}_{-6}		21^{+4}_{-6}		
			31.6	*1.20×10^{-3}*	*27*	*1.28×10^{-3}*	*32*	*3.28*	*9.78*
$^{53}Mn/^{97}Tc$	$>1.70 \times 10^{5}$	59.4	1	1.58×10^{-4}	17^{+2}_{-2}	3.84×10^{-5}	*>7*	1.65×10^{6}	$>2.26 \times 10^{5}$
			31.6	*9.23×10^{-4}*	*26*	*2.04×10^{-4}*	*>17*	*1.82×10^{6}*	*$<2.63 \times 10^{5}$*

Notes. Time and τ_{eq} are in Myr. The ISM $SLR_{1,2}$/stable ratios in Roman are calculated using the steady-state formula from Côté et al. (2019a) and $K = 2.3$. These are cases within Regime I and can provide T_{iso} (also in roman). The ISM $SLR_{1,2}$/stable ratios in italics are calculated instead using the last-event formula, i.e., Equations (3) (with $K = 2.3$) and 4 (with $K = 1.2$) of Côté et al. (2021) and the selected value of $\gamma = \delta$. These are cases within Regime III and can provide T_{LE} (also in italics). The ISM SLR_1/SLR_2 values are calculated as $= P(\tau_1/\tau_2)$ (Equation (7)) for roman values and as $= P$ (Equation (8)) for italic values. The production ratios used in all the formulas are reported in the text in each subsection. The "back-decayed" ratios are calculated by decaying the ESS ratio back by the average of T_{iso}, or T_{LE}, from both $SLR_{1,2}$/stable ratios, except for the case of $^{53}Mn/^{97}Tc$, where only the times derived from ^{53}Mn were used. Differences between the values in the last two columns highlight the problems discussed in the text.
[a] We calculated this possible *r*-process production using the average $^{247}Cm/^{232}Th$ ratio from Goriely & Janka (2016) and assuming the solar ratio $^{127}I/^{232}Th$ of 31 from Asplund et al. (2009). This is to avoid using ^{235}U, which decays much faster than ^{232}Th (with a mean life of roughly 1 Gyr instead of 20 Gyr) and would complicate the assumption that the produced $^{127}I/^{235}U$ was solar.

detailed analysis shown by Côté et al. (2021) demonstrates that there is compatibility for T_{LE} in the range between 100–200 Myr, depending on the exact choice of the K parameter (Côté et al. 2019a), γ, and the production ratios. The short mean lives of ^{247}Cm and ^{129}I ensure that there is no memory from previous events, while the long τ_{eq} of $^{247}Cm/^{129}I$ instead ensures that this ratio did not change significantly during T_{LE} and has a high probability to be within the 10% of the production ratio. Therefore the production ratio of the last *r*-process event that polluted the ESS material can be accurately determined directly from the ESS ratio. If we assume that the last event produced a $^{247}Cm/^{232}Th$ ratio similar to the average predicted by Goriely & Janka (2016) and assume a solar ratio for $^{127}I/^{232}Th$, then we find an inconsistency between the numbers in the last two columns of Table 3. The back-decayed value is more than five times lower than the assumed production ratio, which indicates a weaker production of the actinides from this last event with respect to the production ratios that we are using here. The number in the last column therefore represents a unique constraint on the nature of the astrophysical sites of the *r* process in the Galaxy at the time of the formation of the Sun and needs to be compared directly to different possible astrophysical and nuclear models (Côté et al. 2021).

4.2. The Ratio of the s-process ^{107}Pd and ^{182}Hf

If T_{LE} for the last *r*-process event is longer than 100 Myr, as discussed in the previous section, the presence of these two SLRs in the ESS should primarily be attributed to the slow neutron-capture (*s*) process in asymptotic giant branch (AGB) stars, which are a much more frequent event due to the low mass of their progenitors because their *r*-process contribution would have decayed for a time of about 10 times their mean lives (Lugaro et al. 2014). Experimental results on the SLRs ^{107}Pd ($\tau = 9.8$ Myr) and ^{182}Hf ($\tau = 12.8$ Myr) are reported with respect to the stable reference isotopes ^{108}Pd and ^{180}Hf, respectively. The ISM ratios reported in Table 3 are calculated using production ratios of 0.14, 0.15, and 3.28 for $^{107}Pd/^{108}Pd$, $^{182}Hf/^{180}Hf$, and $^{107}Pd/^{182}Hf$, respectively, derived from the 3 $M_\odot$ model of Lugaro et al. (2014). For the short γ values considered in Table 3 (1 and 3.16 Myr), the $SLR_{1,2}$/Stable ratios belong to Regime I and the SLR_1/SLR_2 ratio belongs to Regime 2. Therefore we can calculate T_{iso} from all the ratios. As shown in Table 2, the ratios relative to the stable reference isotopes have larger uncertainties (40% or 85% depending on γ, and assuming no uncertainty on the stable isotope abundance) compared to the ratio of the two SLRs (less than 20%). However, when the actual ISM ratios are considered, the uncertainties on the evaluation of T_{iso} become comparable because they are relative uncertainties and the ratio of the two SLRs and the equivalent mean life have a much higher absolute value than the other two ratios. While the T_{iso} values derived from the $SLR_{1,2}$/stable ratios are consistent with each other, the value calculated from SLR_1/SLR_2 would need to be much shorter. In the last column of Table 3 we report the back-decayed ratio as the ISM ratio that is required to obtain a self-consistent solution.

The discrepancy between the ISM and back-decayed values may be due to problems with the stellar production of these isotopes: a main caveat to consider here is that while the $^{107}Pd/^{108}Pd$ ratio produced by the *s* process is relatively constant because it only depends on the inverse of the ratio of the neutron-capture cross sections of the two isotopes, both the $^{182}Hf/^{180}Hf$ and $^{107}Pd/^{182}Hf$ production ratios can vary significantly between different AGB star sources. The $^{182}Hf/^{180}Hf$ ratio is particularly sensitive to the stellar mass (Lugaro et al. 2014) due to the probability of activating the ^{181}Hf branching point, which increases with the neutron density produced by the $^{22}Ne(\alpha, n)^{25}Mg$ neutron source reaction, which in turn increases with temperature and therefore stellar mass. The $^{107}Pd/^{182}Hf$ involves two isotopes belonging to the mass region before (^{107}Pd) and after (^{182}Hf) the magic neutron number of 82 at Ba, La, and Ce. This means that this ratio will also be affected by the total number of neutrons released by the main neutron source $^{13}C(\alpha, n)^{16}O$ in AGB stars, which has a strong metallicity dependence (see, e.g., Gallino et al. 1998; Cseh et al. 2018). This means that a proper analysis of these *s*-process isotopes can only be carried out in the framework of full GCE models, where the stellar yields are varied with mass

and metallicity. This work is submitted (Trueman et al. 2021, submitted), and the uncertainties calculated here will be included in this complete analysis.

For long γ values, such as 31.6 Myr considered in Table 3, the $^{107}Pd/^{108}Pd$ and $^{182}Hf/^{180}Hf$ ratios would likely mostly reflect their production in one event only (Regime III). In this case, we derive an T_{LE}. Because $^{107}Pd/^{182}Hf$ is between Regimes 1 and 3, this isotopic ratio changes more significantly during the time interval T_{LE} than in the case of the *r*-process isotopes discussed in the previous section. In Table 3 we report the production value predicted by decaying the ESS ratio back by T_{LE}. As in the case of the *r*-process isotopes, in this regime, this number can be used to determine the stellar yields of the last AGB star to have contributed to the *s*-process elements present in the ESS (Trueman et al. 2021, submitted).

4.3. The Ratio of the p-process ^{97}Tc and ^{98}Tc

These two SLRs are next to each other in mass and are both *p*-only isotopes, i.e., they are nuclei of higher mass than Fe that can only be produced by charged-particle reactions or the disintegration (γ) process. While the origin of *p*-only isotopes is currently not well established especially for those in the light-mass region, and the main sites may be both core-collapse and Type Ia supernova, recent work has shown that the main site of production of the SLRs considered here is probably Chandrasekhar-mass Type Ia supernova (see, e.g., Travaglio et al. 2014; Lugaro et al. 2016; Travaglio et al. 2018). Because their mean lives are remarkably similar ($\tau = 5.94$ and 6.1 Myr, respectively, for ^{97}Tc and ^{98}Tc), their $\tau_{eq} = 226$ Myr and as shown in Table 2, the theoretical uncertainties related to their ratio are very low for values γ up to 31.6 Myr.

The full GCE of these isotopes was investigated by Travaglio et al. (2014). Expanding on that work, in combination with the present results, could provide us with a strong opportunity to investigate both the origin of these *p*-nuclei and the environment of the birth of the Sun. There are many scenarios that might be investigated. If the γ value of the origin site of the Type Ia supernova was around 1 Myr, then we could derive a T_{iso} from all the different ratios and check for self-consistency. If the γ value of the origin site was above 30 Myr, we would instead be in a similar case as the *r*-process isotopes discussed above, and the $^{97}Tc/^{98}Tc$ would give us directly the production ratio in the original site, to be checked against nucleosynthesis predictions. For γ values in between, the $^{97}Tc/^{98}Tc$ ratio would still provide us with the opportunity to calculate T_{iso}. Unfortunately, we only have upper limits for the ESS ratio of these two nuclei, relative to their experimental reference isotope ^{98}Ru, which means that an ESS value for their ratio cannot be given and a detailed analysis needs to be postponed until these data become available.

4.4. The Ratio of ^{97}Tc and ^{53}Mn, also Potentially of Chandrasekhar-mass Type Ia Supernova Origin

From a chemical evolution perspective, the origin of Mn (and therefore ^{53}Mn) is still unclear (Seitenzahl et al. 2013; Cescutti & Kobayashi 2017; Eitner et al. 2020; Kobayashi et al. 2020; Lach et al. 2020). Nevertheless, the $^{53}Mn/^{97}Tc$ ratio can be assumed to be synchronous as there are indications that the main site of origin of ^{53}Mn is the same as that of ^{97}Tc[8] (see, e.g., Lugaro et al. 2016). Table 2 shows that the uncertainty for the ratio of the two SLRs is below 30% for most cases (and as low as 5% when $\gamma = 1$ Myr), while for each one of the individual isotopes it is larger than 60%. Similar to the $^{97}Tc/^{98}Tc$ ratio discussed above, the $^{53}Mn/^{97}Tc$ ratio can also provide the opportunity to investigate T_{iso} for γ values up to 2 Myr because even if $\tau_{eq} = 59.4$ Myr, the shorter mean lives of each SLR do not allow to built a memory, making this a case of Regime 3, which cannot be treated here. The ISM values reported in Table 3 were calculated with a production ratio of 2.39×10^{-2} for $^{97}Tc/^{98}Ru$, 0.108 for $^{53}Mn/^{55}Mn$, and 1.82×10^{6} for $^{53}Mn/^{97}Tc$ (Travaglio et al. 2011; Lugaro et al. 2016).

We obtain potential self-consistent isolation times, mostly determined by the accurate ESS value of $^{53}Mn/^{55}Mn$. Consistency between the last two columns of the table, which could inform us on the relative production of nuclei from nuclear statistical equilibrium (such as ^{53}Mn) and nuclei from γ-process in Chandrasekhar-mass Type Ia supernova (such as ^{97}Tc), could be found only if the $^{97}Tc/^{98}Ru$ ratio in the ESS was 7.3 times lower than the current upper limit.

Similarly to the *s*-process case described above, for high values of γ (e.g., 31.6 and 100 Myr shown in Table 3), the $^{53}Mn/^{55}Mn$ and $^{97}Tc/^{98}Ru$ ratios would record one event only (Regime III) and the derived T_{LE} are consistent with each other. The value from $^{53}Mn/^{55}Mn$ can then be used to decay the ESS ratio of the $^{53}Mn/^{97}Tc$ back and derive a direct constraint for the last *p*-process event that polluted the solar material. Overall, a more precise ^{97}Tc ESS abundance would allow us to take advantage of the low theoretical uncertainties and give a more accurate prediction of the ISM ratio or the production ratio at the site.

4.5. $^{60}Fe/^{26}Al$

Finally, we consider the case for $^{60}Fe/^{26}Al$. This ratio is of great interest in the literature because both isotopes are produced by core-collapse supernovae (Limongi & Chieffi 2006), and they can be observed with γ-rays (Wang et al. 2007) as well as in the ESS (Trappitsch et al. 2018). There are strong discrepancies between core-collapse supernova yields and observations as the yields typically produce a $^{60}Fe/^{26}Al$ ratio at least three times higher than the γ-ray observations (e.g., Sukhbold et al. 2016), and orders of magnitude higher than the ESS ratio (see the discussion in Lugaro et al. 2018).

We cannot apply our analysis to interpret the γ-ray ration because it is derived by measuring first the total abundance of ^{60}Fe and ^{26}Al separatedly, and then dividing them. In this case, the average abundance ratio is given simply by the ratio of the averages, mixing the ^{60}Fe and ^{26}Al productions from several different events, which do not correspond to our synchronous framework.

When the ESS abundance is considered, however, we can apply our methods because the ESS ratio represents the abundance at one time and place in the ISM, generated by a synchronous set of events. In this case, $\tau_1 = 3.78$ Myr (for ^{60}Fe) and $\tau_2 = 1.035$ Myr (for ^{26}Al) results in $\tau_{eq} = -1.45$ Myr. If we consider a $\gamma = 1$ Myr for the core-collapse supernova-enriching events, we fall somewhere between Regime 2 and 4, with ^{60}Fe and ^{26}Al building memory and almost no memory, respectively, between successive events. As a consequence, when we consider our statistical analysis, the average ISM value given by Equation (10) predicted for the $^{60}Fe/^{26}Al$ ratio is a factor of 3.9 of the production ratio. This is 7% higher than the traditional

[8] And ^{98}Tc, but we prefer to consider ^{97}Tc here because both its mean life and its yields are closer to that of ^{53}Mn.

continuous enrichment steady-state formula $P\tau_1/\tau_2$ (i.e., the limit of Equation (2) when δ_c, $\Delta t \to 0$) used in the literature (see, e.g., Sukhbold et al. 2016) because that gives a factor of 3.65 of the production ratio instead. In conclusion, our analysis does not help to solve the problem that core-collapse supernova yields produce much more ^{60}Fe relative to ^{26}Al than is observed in the ESS.

5. Conclusions and Future Work

We presented a statistical framework to study the uncertainties of ratios of SLRs that were present at the formation time of the solar system. We show that this statistical framework is advantageous because

1. it removes the GCE uncertainties associated with the stable reference isotopes that are often used for ESS ratios (i.e., the value of the parameter K investigated by Côté et al. 2019a);
2. it reduces the stochastic uncertainties, i.e., for ratios of two SLRs, these uncertainties are typically much lower than those of SLR/stable isotopic ratios for equivalent regimes.
3. It allows us to define a Regime 3 for the ratio of two SLRs, which is qualitatively different to the regimes described in Paper I for SLR/stable ratios, and represents the case where each mean life is much shorter than γ, while the equivalent mean life of the ratio of the two SLRs is much longer than γ. In this case, the ratios of the two SLRs allow us to constrain the nucleosynthesis inside the last nucleosynthetic events that contributed the solar system matter.

We have identified four ratios: ^{247}Cm/^{129}I (from the *r* process), ^{107}Pd/^{182}Hf (from the *s* process), ^{97}Tc/^{98}Tc (from the *p* process), and ^{53}Mn/^{97}Tc (potentially from Type Ia supernovae), which can be used effectively to either reduce the uncertainty in the $T_{\rm iso}$ calculation (for relatively low values of γ) or to accurately predict the production ratio for the last event that enriched the ESS (for relatively high values of γ). In particular, the inconsistencies we found (see Table 3) between the production and the ESS ratios both for the ^{247}Cm/^{129}I and the ^{107}Pd/^{182}Hf ratios can be used to constrain the events in the Galaxy that produced the *r*-process isotopes (Côté et al. 2021) and the elements belonging to the first *s*-process peak (Trueman et al. 2021, submitted) at the time of the formation of the Sun.

While here we have only investigated the simpler synchronous enrichment scenario in which the two SLRs are assumed to originate from the same events, in the future, we could also investigate the asynchronous enrichment scenario for particular cases such as the ^{146}Sm/^{244}Pu ratio. For example, ^{146}Sm is a *p* nucleus and ^{244}Pu is produced by the *r* process, therefore γ for the production events of the two isotopes is probably very different. The mean life of ^{244}Pu is 115 Myr, while for ^{146}Sm, two different mean lives are reported: 98 Myr (Kinoshita et al. 2012) and 149 Myr (Marks et al. 2014), for which $\tau_{\rm eq} = 663$ Myr and $\tau_{\rm eq} = 504$ Myr, respectively. Because these values are extremely high, the ^{146}Sm/^{244}Pu ratio may provide an opportunity to predict its value with an uncertainty much lower than when the individual isotopes are considered. Another interesting ratio may be ^{135}Cs/^{60}Fe, with a $\tau_{\rm eq} = 26$ Myr (from mean lives of 3.3 and 3.78 Myr, respectively). For a frequent enrichment rate ($\gamma \sim 1$ Myr), the relative uncertainty on the predicted abundance ratio in a synchronous scenario is 4.5%. However, ^{135}Cs is a product of both the *s* and the *r* processes, while ^{60}Fe is ejected mostly by core-collapse supernovae, which would require a complex asynchronous scenario. Furthermore, only an upper limit for the ESS abundance for ^{135}Cs is available.

In general, improvements in ESS data for any of the SLRs considered here will help us to constrain the stellar nucleosynthesis models. Particularly, these improvements are strongly needed for the *p*-process isotopes ^{97}Tc and ^{98}Tc, for which we currently only have upper limits for their ESS abundances. Together with the well-known ^{53}Mn, these SLRs could provide unique constrains on both galactic *p*-process nucleosynthesis and the origin of solar system matter.

We thank the anonymous referee for the careful reading of the paper. This research is supported by the ERC Consolidator Grant (Hungary) funding scheme (Project RADIOSTAR, G.A. n. 724560). B.C. acknowledges the support from the National Science Foundation (NSF, USA) under grant No. PHY-1430152 (JINA Center for the Evolution of the Elements). B.C. and M.L. acknowledge the support from the Hungarian Academy of Sciences via the Lendület project LP2014-17.

Appendix
Calculation of M_1/M_2 Average and Standard Deviation for the Case when δ Is not a Constant

We can define the value of M_1/M_2 by parts as a function of time with

$$\frac{M_1}{M_2} = P\sum_{i=1}^{n} R_i(t), \tag{A1}$$

with

$$R_i(t) = \frac{e^{-t/\tau_1} + \sum_{k=0}^{i-2} e^{-(t-\sum_{m=0}^{k}\delta_m)/\tau_1}}{e^{-t/\tau_2} + \sum_{k=0}^{i-2} e^{-(t-\sum_{m=0}^{k}\delta_m)/\tau_2}}, \tag{A2}$$

where $\delta_{i-1} < t$. Alternatively, $R_i(t)$ can be written as

$$R_i(t) = e^{-t/\tau_{\rm eq}} C_i = e^{-t/\tau_{\rm eq}} \frac{1 + \sum_{k=0}^{i-2} e^{\sum_{m=0}^{k}\delta_m/\tau_1}}{1 + \sum_{k=0}^{i-2} e^{\sum_{m=0}^{k}\delta_m/\tau_2}}. \tag{A3}$$

By using Equation (A3) with $P = 1$, the expression for the average value of M_1/M_2 is simply

$$\left\langle \frac{M_1}{M_2} \right\rangle = \frac{1}{n\langle\delta\rangle} \sum_{i=1}^{n} C_i \int_{\sum_{m=0}^{i-2}\delta_m}^{\sum_{m=0}^{i-1}\delta_m} e^{-t/\tau_{\rm eq}} dt, \tag{A4}$$

from where

$$\left\langle \frac{M_1}{M_2} \right\rangle = \frac{\tau_{\rm eq}}{n\langle\delta\rangle} \sum_{i=1}^{n} C_i \times \left(e^{-\sum_{m=0}^{i-2}\delta_m/\tau_{\rm eq}} - e^{-\sum_{m=0}^{i-1}\delta_m/\tau_{\rm eq}}\right). \tag{A5}$$

From the definition of C_i, we can rewrite the average as

$$\left\langle \frac{M_1}{M_2} \right\rangle = \frac{\tau_{\rm eq}}{n\langle\delta\rangle} \sum_{i=1}^{n} \frac{1 + \sum_{k=0}^{i-2} e^{-\sum_{m=k}^{i-2}\delta_m/\tau_1}}{1 + \sum_{k=0}^{i-2} e^{-\sum_{m=k}^{i-2}\delta_m/\tau_2}} (1 - e^{-\delta_{i-1}/\tau_{\rm eq}}) = \frac{\tau_{\rm eq}}{n\langle\delta\rangle} \sum_{i=1}^{n} S_i (1 - e^{-\delta_{i-1}/\tau_{\rm eq}}). \tag{A6}$$

Alternatively, by taking the averages,

$$\mu = \left\langle \frac{M_1}{M_2} \right\rangle = \frac{\tau_{\rm eq}}{\langle \delta \rangle} (\langle S \rangle - \langle S e^{-\delta/\tau_{\rm eq}} \rangle). \tag{A7}$$

We can obtain a more intuitive expression by approximating

$$\langle S e^{-\delta/\tau_{\rm eq}} \rangle \approx \langle S \rangle \langle e^{-\delta/\tau_{\rm eq}} \rangle, \tag{A8}$$

and

$$\langle S \rangle \approx \frac{1 - \langle e^{-\delta/\tau_2} \rangle}{1 - \langle e^{-\delta/\tau_1} \rangle}, \tag{A9}$$

from which we can obtain that

$$\mu = \left\langle \frac{M_1}{M_2} \right\rangle \approx \frac{\tau_{\rm eq}}{\langle \delta \rangle} \frac{1 - \langle e^{-\delta/\tau_2} \rangle}{1 - \langle e^{-\delta/\tau_1} \rangle} (1 - \langle e^{-\delta/\tau_{\rm eq}} \rangle). \tag{A10}$$

In order to calculate the standard deviation, we have to obtain the expression for the average of $(M_1/M_2)^2$. Following similar steps as before, we find that

$$\left\langle \left(\frac{M_1}{M_2} \right)^2 \right\rangle = \frac{\tau_{\rm eq}}{2\langle \delta \rangle} (\langle S^2 \rangle - \langle S^2 e^{-2\delta/\tau_{\rm eq}} \rangle). \tag{A11}$$

From Equations (A7) and (A11), we can calculate the exact standard deviation as

$$\sigma = \sqrt{\left\langle \left(\frac{M_1}{M_2} \right)^2 \right\rangle - \left\langle \frac{M_1}{M_2} \right\rangle^2}. \tag{A12}$$

However, in the interest of having a more intuitive expression, we can approximate

$$\langle S^2 \rangle \approx \frac{(1 + \langle e^{-\delta/\tau_1} \rangle)(1 - \langle e^{-2\delta/\tau_2} \rangle)(1 - \langle e^{-\delta/\tau_2} \rangle)}{(1 + \langle e^{-\delta/\tau_2} \rangle)(1 - \langle e^{-2\delta/\tau_1} \rangle)(1 - \langle e^{-\delta/\tau_1} \rangle)}, \tag{A13}$$

from which we can obtain the final expression,

$$\frac{\sigma}{\mu} \approx \sqrt{\frac{\langle \delta \rangle}{2\tau_{\rm eq}} \frac{1 - \langle e^{-2\delta/\tau_{\rm eq}} \rangle}{(1 - \langle e^{-\delta/\tau_{\rm eq}} \rangle)^2} - 1}. \tag{A14}$$

ORCID iDs

Andrés Yagüe López https://orcid.org/0000-0002-7294-9288
Benoit Côté https://orcid.org/0000-0002-9986-8816
Maria Lugaro https://orcid.org/0000-0002-6972-3958

References

Anglés-Alcázar, D., Faucher-Giguère, C.-A., Kereš, D., et al. 2017, MNRAS, 470, 4698
Asplund, M., Grevesse, N., Sauval, A. J., & Scott, P. 2009, ARA&A, 47, 481
Bartos, I., & Marka, S. 2019, Natur, 569, 85
Bland-Hawthorn, J., & Gerhard, O. 2016, ARA&A, 54, 529
Cescutti, G., & Kobayashi, C. 2017, A&A, 607, A23
Clayton, D. D. 1984, ApJ, 285, 411
Côté, B., Eichler, M., Yagüe, A., et al. 2021, Sci, 371, 945
Côté, B., Lugaro, M., Reifarth, R., et al. 2019a, ApJ, 878, 156
Côté, B., Yagüe, A., Világos, B., & Lugaro, M. 2019b, ApJ, 887, 213
Cseh, B., Lugaro, M., D'Orazi, V., et al. 2018, A&A, 620, A146
Dauphas, N., & Chaussidon, M. 2011, AREPS, 39, 351
de Avillez, M. A., & Mac Low, M.-M. 2002, ApJ, 581, 1047
Diehl, R., Lang, M. G., Martin, P., et al. 2010, A&A, 522, A51
Eitner, P., Bergemann, M., Hansen, C. J., et al. 2020, A&A, 635, A38
Fujimoto, Y., Krumholz, M. R., & Tachibana, S. 2018, MNRAS, 480, 4025
Gallino, R., Arlandini, C., Busso, M., et al. 1998, ApJ, 497, 388
Goriely, S., & Janka, H. T. 2016, MNRAS, 459, 4174
Hotokezaka, K., Piran, T., & Paul, M. 2015, NatPh, 11, 1042
Huss, G. R., Meyer, B. S., Srinivasan, G., Goswami, J. N., & Sahijpal, S. 2009, GeCoA, 73, 4922
Kinoshita, N., Paul, M., Kashiv, Y., et al. 2012, Sci, 335, 1614
Kobayashi, C., Leung, S.-C., & Nomoto, K. 2020, ApJ, 895, 138
Lach, F., Röpke, F. K., Seitenzahl, I. R., et al. 2020, A&A, 644, A118
Limongi, M., & Chieffi, A. 2006, ApJ, 647, 483
Lodders, K. 2010, ASSP, 16, 379
Lugaro, M., Heger, A., Osrin, D., et al. 2014, Sci, 345, 650
Lugaro, M., Ott, U., & Kereszturi, Á. 2018, PrPNP, 102, 1
Lugaro, M., Pignatari, M., Ott, U., et al. 2016, PNAS, 113, 907
Marks, N. E., Borg, L. E., Hutcheon, I. D., Jacobsen, B., & Clayton, R. N. 2014, E&PSL, 405, 15
Meyer, B. S., & Clayton, D. D. 2000, SSRv, 92, 133
Naab, T., & Ostriker, J. P. 2017, ARA&A, 55, 59
Pleintinger, M. M. M., Siegert, T., Diehl, R., et al. 2019, A&A, 632, A73
Seitenzahl, I. R., Cescutti, G., Röpke, F. K., Ruiter, A. J., & Pakmor, R. 2013, A&A, 559, L5
Somerville, R. S., & Davé, R. 2015, ARA&A, 53, 51
Sukhbold, T., Ertl, T., Woosley, S. E., Brown, J. M., & Janka, H. T. 2016, ApJ, 821, 38
Trappitsch, R., Boehnke, P., Stephan, T., et al. 2018, ApJL, 857, L15
Travaglio, C., Gallino, R., Rauscher, T., et al. 2014, ApJ, 795, 141
Travaglio, C., Rauscher, T., Heger, A., Pignatari, M., & West, C. 2018, ApJ, 854, 18
Travaglio, C., Röpke, F. K., Gallino, R., & Hillebrandt, W. 2011, ApJ, 739, 93
Tsujimoto, T., Yokoyama, T., & Bekki, K. 2017, ApJL, 835, L3
Tumlinson, J., Peeples, M. S., & Werk, J. K. 2017, ARA&A, 55, 389
Wallner, A., Faestermann, T., Feige, J., et al. 2015, NatCo, 6, 5956
Wang, W., Harris, M. J., Diehl, R., et al. 2007, A&A, 469, 1005